

# Neurostream: Scalable and Energy Efficient Deep Learning with Smart Memory Cubes

Erfan Azarkhish, Davide Rossi, Igor Loi, and Luca Benini, *Fellow, IEEE*

**Abstract**—High-performance computing systems are moving toward 2.5D as in High Bandwidth Memory (HBM) and 3D integration of memory and logic as in Hybrid Memory Cube (HMC) to mitigate the main memory bottlenecks. This trend is also creating new opportunities to revisit near-memory computation. In this paper, we propose a flexible processor-in-memory (PIM) solution for scalable and energy-efficient execution of deep convolutional networks (ConvNets), one of the fastest-growing workloads for servers and high-end embedded systems. Our co-design approach consists of a network of Smart Memory Cubes (modular extensions to the standard HMC) each augmented with a many-core PIM platform called NeuroCluster. NeuroClusters have a modular design based on NeuroStream floating-point (FP) co-processors (for Convolution-intensive computations) and general-purpose RISC-V cores. In addition, a DRAM-friendly tiling mechanism and a scalable programming paradigm are presented to efficiently harness this computational capability with a very low programming effort. NeuroCluster occupies only 8% of the total logic-base (LoB) die area in a standard HMC and achieves an average performance of 240 GFLOPS for complete execution of full-featured state-of-the-art (SoA) ConvNets within a power budget of 2.5 W. An energy efficiency of 22.5 GFLOPS/W is achieved in a single 3D stack which is 5X better than the best off-the-shelf GPU implementation. The minor increase in system-level power and the negligible area increase make our PIM system a cost effective and energy efficient solution, easily scalable to 955 GFLOPS with a network of four SMCs.

**Index Terms**—Hybrid Memory Cube, Convolutional Neural Networks, Large-scale Deep Learning, Streaming Floating-Point

## I. INTRODUCTION

Today brain-inspired computing (BIC) is successfully used in a wide variety of applications such as surveillance, robotics, industrial, medical, and entertainment systems. Convolutional neural networks (ConvNets) are known as the SoA machine learning (ML) algorithms specialized at BIC, loosely inspired by the organization of the human brain [1]. ConvNets process raw data directly, combining the classical models of feature extraction and classification into a single algorithm. This combination is realized by several simple linear/non-linear

E. Azarkhish, D. Rossi, and I. Loi are with the Department of Electrical, Electronic and Information Engineering, University of Bologna, 40136 Bologna, Italy (e-mails: {erfan.azarkhish, davide.rossi, igor.loi}@unibo.it).

L. Benini is with the Department of Information Technology and Electrical Engineering, Swiss Federal Institute of Technology Zurich, 8092 Zurich, Switzerland, and also with the Department of Electrical, Electronic and Information Engineering, University of Bologna, 40136 Bologna, Italy (e-mail: lbenini@iis.ee.ethz.ch).

This project has received funding from the European Unions Horizon 2020 research and innovation programme under grant agreement No 732631; Swiss National Science Foundation under grant 162524 (MicroLearn: Micropower Deep Learning), armasuisse Science & Technology; and the ERC MultiTher-man project (ERC-AdG-291125).

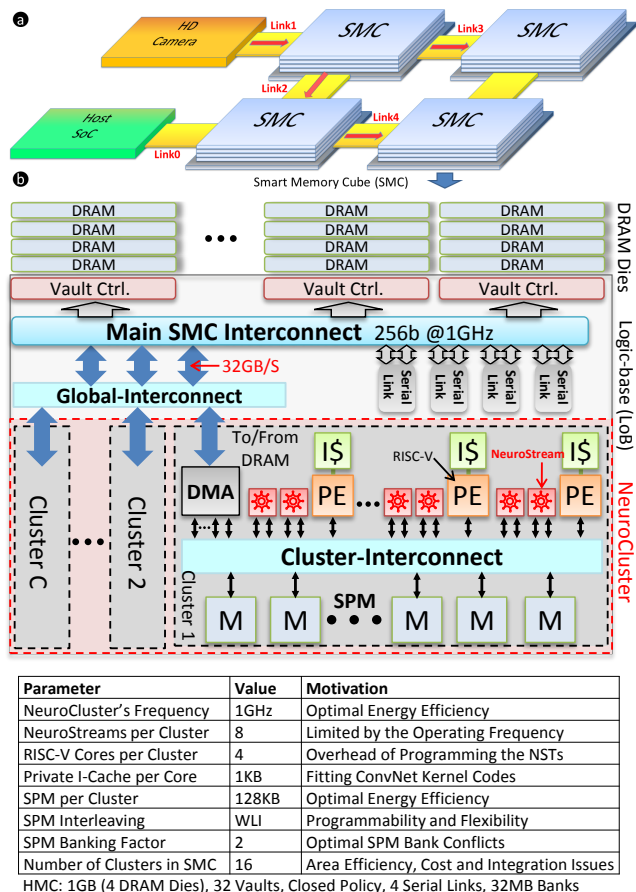


Fig. 1. (a) An overview of the SMC-network for scalable ConvNet execution, (b) block diagram of one SMC instance highlighting the NeuroCluster platform along with the baseline system parameters.

layers transforming the representation into higher and more abstract levels [2]. Typical ConvNet layers include convolutional (CONV), activation (ACT), pooling (POOL), and fully-connected (FC) layers with different characteristics and parameters [1] [2]. The first layer connects the ConvNet to its input volume (an image, a video frame, or a signal, depending on the application). The CONV layer is the core building block of the ConvNets doing most of the computational heavy-lifting, with the main purpose to extract features from the inputs. From the implementation point of view, CONV is a 2/3D convolution over the input volume relying on the Multiply-and-accumulate (MAC) operation [1]. After each CONV layer, a non-linear activation function (e.g. sigmoid, tanh, or ReLU [3]) is performed on each individual neuron. This non-linearity gives the neural-networks superior classification and learning

capabilities over linear classifiers and allows them to solve non-trivial problems [2]. It is common to periodically insert a POOL layer in-between successive CONV layers in a ConvNet architecture. Its function is to progressively reduce the spatial size of the representation to reduce the amount of parameters and computation in the network, and hence to also control over-fitting [4]. The POOL Layer operates independently on every depth slice of the input and resizes it spatially, using the *Max* operation [1]. In the final layers, multiple FC layers perform the final classification and transform the results into several classes. FC layers have a full connectivity and work similar to multi-layer perceptrons (MLPs). Compared to the rest of the network, their computational complexity is usually very small [1] [5]. As will be shown later in Figure 3a,b, a ConvNet is identified by  $l$  layers, each of which can be CONV+ACT, POOL, or FC. Each layer has  $C_i$  input channels of width  $X_i$  and height  $Y_i$ , being transformed into  $(X_o, Y_o, C_o)$  outputs. This terminology is used throughout this paper.

The key advantage of ConvNets over traditional MLPs is local connectivity. When dealing with high-dimensional inputs such as images, it is impractical to connect neurons to all neurons in the previous layer. Instead, each neuron is connected to only a local region of the previous layer (or the input volume) called its receptive field [6]. This can be translated into a convolution operation with a small filter size. It is worth mentioning that ConvNets are not only limited to image-processing and they can be applied to other workloads such as audio [7], video [8], and even RFID-based activity recognition in [9]. Also, scientific workloads such as function approximation [10] and particle search [11] are another important target for ConvNets, motivating the need for a highly scalable and energy efficient execution platform for them. In addition, recurrent and spiking NNs (RNN and SNN) have been recently utilized for deep learning and implemented on scalable network-on-chips [12] [13] [14]. These networks have a great potential for solving time-dependent pattern recognition problems because of their inherent dynamic representations. All these emerging deep-learning models can be future targets for our PIM proposal, yet, in this paper we focus on ConvNets for image and video. Recently, several research programs have been launched, even by major global industrial players (e.g. Facebook, IBM, Google, Microsoft), pushing towards deploying services based on brain-inspired ML to their customers [15] [16] [17]. These companies are interested in running such algorithms on powerful compute clusters in large data centers.

A diverse range of ConvNet implementations exist today ranging from standard software libraries running on general-purpose platforms [18] [19] [20] to application-specific FPGA [21] [22] [23] [24] and ASIC implementations [25] [26] [27] [28]. High-performance supercomputers such as NVIDIA DGX-1 [29] based on Pascal GPU architecture and NVIDIA Tesla K40 [30] also high-end co-processors such as Intel Xeon Phi [31] provide a significant processing power with over 100 W power consumption. Given their enormous processing capabilities, these platforms are the prevailing solutions for offline training and large-scale applications. In this paper, we will demonstrate an alternative solution which is able to

achieve a similar performance with more than 4X reduction in the power consumption compared to the best GPU implementations.

Application-specific implementations achieve a high energy efficiency with the possibility to target embedded domains [24] [25] [27]. However, with the recent growth in the computation and storage requirements of modern ConvNets, pure application-specific solutions are facing challenges limiting their applicability to smaller networks [32]. This is while here we target scalable and flexible execution of deep ConvNets with growing memory footprints. Another common approach is to augment a RISC processor with a SIMD-like extension. In [33] a Tensilica processor is extended with a Convolution Engine. Commercial platforms following a similar trend include TI AccelerationPAC [34], CEVA-XM4 [35], Synopsys DesignWare EV5x, and Movidius Fathom [36]. Movidius Myriad-2 [37], used in Google Tango and the Mobileye EyeQ3, follows a similar approach. Performance and efficiency characterization of these platforms is not publicly available, nevertheless, SIMD extensions require more programming effort to be efficiently utilized, and their register-file bottleneck limits their scalability [26]. In this paper, we follow a different approach based on many scalar co-processors working in parallel on a shared memory. This is described in section III.

Even though, ConvNets are computation-intensive workloads, their scalability and energy efficiency are ultimately bound by the main memory where their parameters and channels need to be stored because of their large size. For example ResNet-152 [38] requires more than 200MB of storage as described later in subsection II-A. For this reason, improving the performance and efficiency of ConvNet accelerators, without consideration of the memory bottlenecks can lead to incorrect decisions. Heterogeneous Three-Dimensional (3D) integration is helping mitigate the well-known memory-wall problem [39]. The Through-silicon-via (TSV) technology is reaching commercial maturity by memory manufacturers [39] (DRAM [40] and flash [41]) to build memory cubes made of vertically stacked thinned memory dies in packages with smaller footprint and power compared with traditional multi-chip modules, achieving higher capacity. On the other hand, a new opportunity for revisiting near-memory computation to further close the gap between processors and memories has been provided in this new context [42] by 3D integration of logic and memory in their own optimized process technologies. This approach promises significant energy savings by avoiding energy waste in the path from processors to memories. In 2013, an industrial consortium backed by several major semiconductor companies standardized the hybrid memory cube (HMC) [40] as a modular and abstracted 3D memory stack of multiple DRAM dies placed over a logic base (LoB) die, providing a high-speed serial interface to the external world. More recently, a fully backward compatible extension to the standard HMC called the smart memory cube (SMC) has been introduced in [43], augmenting the LoB die with generic PIM capabilities. In [44], also, a flexible programming model for SMC has been developed for offloading user level tasks, through standard drivers and APIs including full support for paged virtual memory [44].

TABLE I  
STORAGE REQUIREMENT (MB) IN THE SOA CONVNETS.

| ConvNet   | Max<br>(Neurons/Layer) | Max<br>(Coeffs./Layer) | Max<br>(Storage/Layer) | Total<br>Coeffs. | Total<br>(MB) |
|-----------|------------------------|------------------------|------------------------|------------------|---------------|
| AlexNet   | 2 (MB)                 | 5                      | 6                      | 14               | 16            |
| ResNet50  | 4                      | 9                      | 9                      | 79               | 83            |
| ResNet101 | 4                      | 9                      | 9                      | 151              | 155           |
| ResNet152 | 4                      | 9                      | 9                      | 211              | 214           |
| VGG16     | 25                     | 9                      | 25                     | 56               | 81            |
| VGG19     | 25                     | 9                      | 25                     | 76               | 101           |
| GoogLeNet | 4                      | 4                      | 4                      | 19               | 23            |
| 250K      | 19                     | 9                      | 19                     | 228              | 247           |
| 1M        | 76                     | 9                      | 76                     | 245              | 321           |
| 2M        | 150                    | 9                      | 150                    | 262              | 411           |
| 4M        | 305                    | 9                      | 305                    | 279              | 584           |

In this paper, we design a scalable and energy-efficient platform targeting flexible execution of deep ConvNets with growing memory footprints and computation requirements. Our proposal requires only 8% of the total LoB die area in a standard HMC [40] and achieves 240 GFLOPS on average for complete execution of full-featured ConvNets within a power-budget of 2.5 W. 22.5 GFLOPS/W energy efficiency is achieved in the whole 3D stack which is 5X better than the best GPU implementation [30]. We also demonstrate that using an efficient tiling mechanism along with a scalable programming model it is possible to efficiently utilize this platform beyond 90% of its roofline [45] limit, and scale its performance to 955 GFLOPS with a network of four SMCs.

This paper is organized as follows. Related research efforts are presented in section II. Our architectural design methodology and computation model are explained in section III and section IV, respectively. The programming paradigm is presented in section V. Experimental results are in section VI, and conclusions and future directions are explained in section VII.

## II. RELATED WORK

This section presents the related research efforts in this field. subsection II-A describes the evolution of modern ConvNets and their uprising implementation challenges. subsection II-B presents the existing implementations for them, comparing them with this work.

### A. Implementation Challenges of Modern ConvNets

ConvNets have been rapidly evolving in the past years, from small networks of only a few layers [32] to over hundred [38] and thousand [46] layers, and from having a few kilo-bytes of coefficients (a.k.a. weights) to multi-mega bytes in [6] [15] [38]. Also, traditional ConvNets were only applicable to small 32x32 images, while the SoA ConvNets have 224x224 inputs, and this size is expected to grow [2].

Table I shows an estimation for the storage requirements (in MB) of top-performing ConvNets, assuming layer-by-layer execution. AlexNet [47] is the 2012 winner of the LSVRC challenge [48]. VGG networks [49] and GoogLeNet [15] were the winners of different categories in 2014, and ResNet [38] was the most recent winner of this challenge in 2015. ResNet1K with 1001 layers [46] is omitted from our study because its training loss and validation error (for the ImageNet database [48]) are not yet lower than its previous

versions. Instead in this paper, ResNet-152 has been extended to larger networks (accepting 250K/1M/2M/4M-pixel images shown in Table I), to further investigate the scalability of our approach and its applicability to beyond High-Definition (HD) image resolutions. It can be clearly seen that the typical on-chip (L1, L2) storages in the memory hierarchy (caches or SRAM-based scratchpad memories) cannot accommodate even a single layer of these ConvNets, as the required storages per layer range from 6 MB to over 300 MB. In addition, the assumption that all coefficients can be stored on-chip ([50] [51] [28] [25]) is not valid anymore, as an additional storage of 14~280 MB is required to accommodate the coefficients. Overall, 16~580 MB is required for layer-by-layer execution, demonstrating that DRAM is necessary as the main storage for deep ConvNets. A similar observation was recently made in [52].

Another point is that the straightforward topology of the traditional ConvNets such as LeNet-5 [32] has recently evolved to more complex topologies such as Deep Residual Learning in ResNet [38] and the Inception Model (Network in Network) in GoogLeNet [15]. This makes application specific implementations less practical and highlights the need for flexible and programmable platforms. Also, unlike traditional ConvNets with very large and efficient convolution filters (a.k.a. feature maps) of over 10x10 inputs, modern ConvNets tend to have very small filters (e.g. 3x3 in VGG and 1x1 in GoogLeNet and ResNet). It can be easily verified that the Operational Intensity (OI)<sup>1</sup> decreases as the convolution filters shrink. This can negatively impact computation, energy, and bandwidth efficiency of the implementations (See section VI). In this paper, we design a scalable PIM platform capable of running very deep networks with large input volumes and arbitrary filter sizes.

Lastly, different tiling methods for ConvNets have been previously used in [22] and [53] for an FPGA implementation, in [51] for a neuromorphic accelerator, and in [54] for a Very Long Instruction Word (VLIW) architecture. In [54] a tile-strip mechanism is proposed to improve locality and inter-tile data reuse for ConvNets with large filters. Also, tile-aware memory layouts have been previously proven effective for multi-core [55] and GPU implementations [56] of linear algebra algorithms, directly affecting their cache performance, bandwidth efficiency, and the degree of parallelism. In this paper, we introduce a more general and flexible form called 4D-tiling (subsection IV-A) allowing for optimization of performance and energy efficiency under given constraints such as on-die SPM and DRAM bandwidth usage.

### B. SoA ConvNet Implementations

A glance at the existing ConvNet implementations highlights two main directions: (I) Application-specific architectures based on ASIC/FPGAs [25] [24] [27] [51]; (II) Software implementations on programmable general-purpose platforms

<sup>1</sup>Operational Intensity (OI), a.k.a. Computation to Communication Ratio, is a measure of computational efficiency defined in the roofline-model [45] as the number of computations divided by the total transferred data.

such as CPUs and GPUs [5] [30] [22]. FPGA/ASIC implementations achieve impressive energy efficiency and performance: DianNao [51] achieves 450 GFLOPS at 0.5 W with a neuromorphic architecture using 16b fixed-point arithmetic in 65nm technology. Later, it has been extended to 1250 GFLOPS within a similar power budget in [57]. The limiting assumption in this work is that the whole ConvNet (coefficients + the largest intermediate layer of LeNet-5) fits inside the on-chip SRAM ( $\sim 256\text{KB}$ ). As we showed above, this assumption is not valid anymore for modern ConvNets. Also, they use a small input image size (32x32) with very large convolution filters (e.g. 18x18, 7x7), which is unrealistic for modern ConvNets, as explained before. EIE [50] achieves 100 GFLOPS at 625 mW in 45nm technology, with the main drawback of storing 84M coefficients on-chip, resulting in an area of over  $40\text{mm}^2$ . In [25] an ASIC implementation of NeuFlow in IBM 45nm SOI technology with an area of  $12.5\text{mm}^2$  is presented. It achieves 300 GFLOPS at 0.6 W, operating at 400 MHz. Later this work has been ported to Xilinx Xynq-ZC706 in nn-X [24], achieving 227 GFLOPS at 9 W. Finally, Origami [27] achieves 145 GFLOPS at 0.5 W, using 12b fixed-point implementation (65nm-UMC @1.2V technology at 1.2V, with 40KB of storage), being scalable to 800 GFLOPS/W at 0.8V. The main issue with all these works is their lack of flexibility and adaptivity to large inputs and modern ConvNets. Also, the assumption that a significant part of the ConvNet can be stored on-chip is not valid anymore, and shrinking filter dimensions can significantly hurt their reported performance and efficiency numbers with 18x18 filters in [51], 10x10 in [24] [25], 7x7 in [52], and 6x6 in [27]. due to the significantly reduced OI.

General-purpose CPU/GPU platforms, on the other hand, are able to flexibly execute different deep neural networks [30] [5] [22] without the limitations of application specific architectures. Fast and user-friendly frameworks such as Torch [18], CAFFE [19], and cuDNN [20] are publicly available which also provide facilities to efficiently train deep NNs. In [30] over 500 GFLOPS has been reported for execution of the CAFFE models based on cuDNN on NVIDIA Tesla K40 with default settings. By turning off error-correction and boosting the clock speed they have been able to reach 1092 GFLOPS. Assuming a maximum device power of 235 W, an energy efficiency of 4.6 GFLOPS/W can be estimated for it. Geforce GTX 770 achieves an energy efficiency of around 2.6 GFLOPS/W using the same framework [30]. The NVIDIA DGX-1 supercomputer can achieve 170 TFLOPS [29] with half-precision floating-point (FP). This boost comes from the new Pascal GPU architecture and the leading edge technology of 14nm. No data about the performance and energy of executing ConvNets on it is available, yet. Mobile GPUs achieve similar energy efficiencies at lower power budgets. 54 GFLOPS for less than 30 W is reported in [25] for NVIDIA GT335M, and in [5] 84 GFLOPS for 11 W is reported for NVIDIA Tegra K1. CPU implementations achieve lower energy efficiency. In [22], 12.8 GFLOPS at 95 W has been reported for Intel Xeon CPU E5-2430 (@2.20GHz) with 15MB cache and 16 threads. In [5], 35 GFLOPS at 230 W has been reported for Intel Xeon E5-1620v2. In [26] a domain-specific instruction set architecture (ISA) is designed for the widely used neural

network (NN) models by identifying the common operations in them. They show higher flexibility compared to [51] by being able to model 9 classes of NNs. The size of the studied networks, however, are extremely small compared to the ones studied in our paper.

On the other hand, Google's TensorFlow platform [58] maps large scale ML problems to several machines and computation devices, including multi-core CPUs, general-purpose GPUs, and custom designed ASICs known as Tensor Processing Units (TPUs). Nervana, also, has built a scalable ML platform [59] with their own implementation of TPUs, and a library called Neon to support cloud computation with different backends. Apache Spark features an ML library called MLlib [60] targeting scalable practical ML. No performance or efficiency data is publicly available for these platform. HCL2 [61] motivates designing a heterogeneous programming system based on map-reduce for ML applications supporting CAFFE [19] representations.

The study of the ConvNets in a near-memory context has been done in [62] [52] [63]. In [62] the authors assume that the whole internal bandwidth of the HMC (320 GB/s) is available to PIM. They target a maximum performance of 160 GFLOPS inside each cube, and the details of their PIM design are not exposed in their work. Plus, instead of performance efficiency, normalized execution time is reported only, and the analysis of power and area are left as future works. In [52] a data-driven computing model is proposed using state-machines near each HMC vault controller, preprogrammed to generate DRAM addresses for the ConvNet under execution. Their study, however, is limited to a small ConvNet with 6 layers and scaling their approach to modern ConvNets seems difficult. They, also, achieve 132 GFLOPS at 3.4 W with an energy efficiency lower compared to our work, mainly due to the presence of data caches, on-chip storage for weights, and network-on-chip routers with packet encapsulation in their accelerator design. Finally, in [63], ConvNet execution in ReRAM based non-volatile memory is investigated with different design decisions due to the drastically different memory technology used. Relative performance and energy numbers reported in this work make it difficult to compare directly, nevertheless, a throughout survey on the techniques to use these memories in comparison with DRAM is presented in [64]. In this paper, we present a general-purpose and resource-aware PIM implementation for large-scale ConvNets, targeting over 240 GFLOPS @22.5 GFLOPS/W. The key features of our solution are the design of a scalable and flexible architecture, providing an energy efficiency higher than the best CPU/GPU implementations. We use 32-bit FP arithmetic with no restrictions to maintain the highest flexibility, yet in subsection VI-A we briefly study the implications of reduced precision arithmetic, as well.

### III. SYSTEM ARCHITECTURE

ConvNets, by nature, are computation demanding algorithms. One forward pass of VGG19, for example, requires around 20 billion MAC operations with over 100K operations per pixel. Maintaining even a frame-rate of 10 frames per second will require over 200 GFLOPS. In theory, ConvNets can

reach extremely high OI ratios (described in subsection II-A), as they reuse data efficiently. However, due to the very large memory footprints of deep ConvNets (See Table I) their performance and energy efficiency is ultimately constrained by the main DRAM storage and off-chip communication. As we will show throughout this paper, in a near-memory context some of these constraints can be relaxed, providing the possibility to achieve higher energy efficiency compared to GPUs and host-side accelerators. subsection III-A describes the design of our many-core PIM platform.

### A. NeuroCluster

NeuroCluster (Illustrated in Figure 1b) is a flexible clustered many-core capable of performing general-purpose computations inside the SMC. It has been designed based on energy-efficient RISC-V processing-elements (PEs) [65] and NeuroStream (NST) floating-point co-processors (described in subsection III-B), all grouped in tightly-coupled clusters. As shown in Figure 1b, each cluster consists of four processors (called PEs) and eight NSTs, with each PE being responsible for programming and coordinating two of the NSTs. This configuration is found to be optimal in the explorations presented in section VI. The PEs are augmented with a light-weight Memory Management Unit (MMU) along with a small sized Translation Look-aside Buffer (TLB) providing zero-copy virtual pointer sharing from the host to NeuroCluster (More information: section V). Instead of caches and prefetchers which provide a higher-level of abstraction without much control, and they are more suitable for host-side accelerators [44], scratchpad memories (SPMs) and DMA engines are used with a simple and efficient programming paradigm to boost energy efficiency [66] [44] [54]. Also, caches introduce several coherence and consistency concerns, and are less area and energy efficient in comparison with SPMs [67].

Each cluster features a DMA engine capable of performing bulk data transfers between the DRAM vaults and the scratchpad memory (SPM) inside that cluster. It supports up to 32 outstanding transactions and accepts virtual address ranges without any alignment or size restrictions. The NST co-processors, on the other hand, have limited visibility only to the cluster’s SPM with no concerns about virtual address translations and DMA transfers. This simple paradigm allows for efficient computation while maintaining the benefits of address translation and virtual memory support.

Each PE is a light-weight RISC-V based processor with 4 pipeline stages and in-order execution (no branch prediction, predication, or multiple issue is supported) for energy efficient operation [65]. Register-Transfer-Level (RTL) models of these cores have been adopted from [68]. 1 KB of private instruction-cache (4-way set associative) beside each PE is enough to fit medium sized computation kernels typical of ConvNet workloads. The SPM inside each cluster is organized in multiple banks accessible through the cluster-interconnect. The cluster-interconnect has been designed based on the logarithmic-interconnect proposed in [69] to provide low-latency all-to-all connectivity inside the clusters. Also, the AXI-4 based global-interconnect, connecting the clusters, follows the same

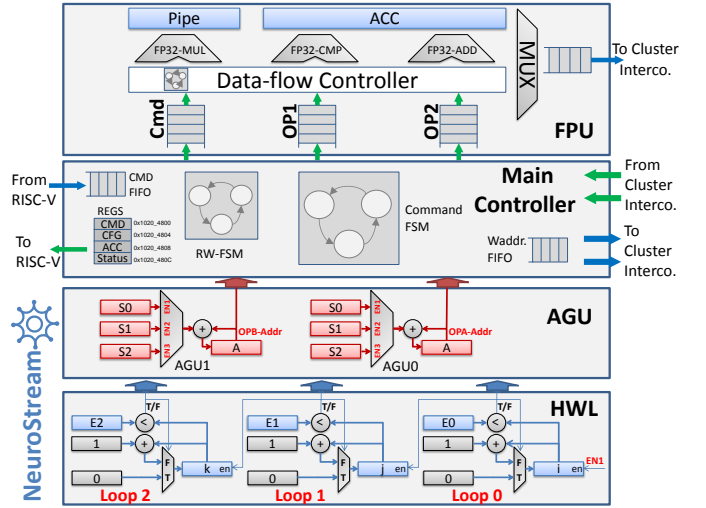


Fig. 2. Architectural diagram of the NeuroStream (NST) floating-point co-processors.

architecture as the SMC-Interconnect [43] to achieve a very high bandwidth.

### B. NeuroStream

NeuroStream (NST) is a streaming co-processor designed based on two observations: (I) Modern ConvNets tend to have very small convolution filters, making coefficient reuse less practical in them (previously discussed in subsection II-A). (II) The most demanding operation in ConvNets is MAC [5]. Therefore, unlike conventional Single-Instruction-on-Multiple-Data (SIMD) co-processors (e.g. ARM NEON), NST works directly on the shared multi-bank SPM without having many internal registers (just one accumulator). This feature along with its dedicated hardware address generators allows it to perform arbitrary computations efficiently and directly on the SPM. This removes the register-file bottleneck which is present in SIMD architectures, and allows it to achieve a performance of 1 FP MAC/cycle. Moreover, each NST can be treated as a scalar co-processor working independently. Yet, it is possible to instantiate several NSTs inside a cluster to achieve a scalable parallelism. This way, NSTs are easier to program compared to SIMD units, and they provide more flexibility in terms of the size/shape/stride of the computations. In total, 128 instances of NST, clocked at a moderate speed of 1 GHz, sum up to 256 GFLOPS of raw performance in the NeuroCluster.

Figure 2 illustrates the block diagram of NST, composed of a main controller, three hardware-loops (HWL), two Address Generation Units (AGUs), and a single-precision floating-point data-path compatible with the IEEE-754 standard. The main-controller is responsible for receiving the commands from the processor and issuing them to the data-path. A parametric-depth first-in-first-out (FIFO) command-queue is implemented to hide the programming latencies. Also, the control interface is memory-mapped, making it possible to communicate with different processors. The hardware-loops are programmable state-machines capable of modeling up to three nested-loops. The AGUs can be programmed to generate complex strided



SPM access patterns (See subsection V-A). By having two direct ports to the cluster-interconnect, each NST can fetch two operands (typically one coefficient and one data) in a single-cycle and perform an operation on them.

NST supports strided convolution, max-pooling, ReLU-activation, along with different forms of gradient-descent for back-propagation and training. Apart from these specialized ConvNet operations, it can also be used for generic computations such as dot product, matrix multiplication, linear transformations, and weighted sum/average. Even single FP operation are supported for generality. More than 14 commands in three categories are implemented: streaming (e.g. *STREAM\_MAC*, *STREAM\_SUM*, *STREAM\_MAX*), single (e.g. *SINGLE\_ADD*, *SINGLE\_MUL*), and memory commands (for configuration and memory transfers to/from the accumulator). subsection V-A describes how NSTs can be programmed to do various computations.

#### IV. COMPUTATION MODEL

When a ConvNet such as GoogLeNet is selected for execution over our PIM system, first it is tiled using the novel 4D-tiling mechanism described in subsection IV-A. This procedure prepares it for parallel execution over the clusters, and optimally partitions it to achieve the highest efficiency under given constraints such as on-die SPM and DRAM bandwidth usage. Next, all coefficients are loaded in SMC’s DRAM and an additional space is reserved there for the intermediate results of the largest layer (see Table I). The input volume (e.g. the image or video frame) is loaded into this area before each run. The actual execution takes place layer-by-layer, each layer being parallelized over 16 clusters. Only at the end of each layer the clusters are synchronized. Each cluster executes one 4D-tile at a time with all its NSTs working cooperatively to compute its final result inside the cluster’s SPM. A more detailed description follows in subsection IV-A and subsection IV-B.

##### A. 4D-Tiling Mechanism

A 4D-tile (illustrated in Figure 3b) is a subset of the input volume (called Input-tile) and output volume (Output-tile) of a convolutional layer ( $l$ ) identified by the  $(T_{X_i}^{(l)}, T_{Y_i}^{(l)}, T_{C_i}^{(l)}, T_{C_o}^{(l)})$  tuple.  $T_{X_i}^{(l)}$  and  $T_{Y_i}^{(l)}$  are the tile width and height of the input volume of layer  $l$ , and  $T_{C_i}^{(l)}$  and  $T_{C_o}^{(l)}$  are the number of input and output channels to the tile). The output dimensions of each tile are calculated directly from input width and height, filter dimensions, striding, and zero-padding parameters. 4D-tiles have three main features essential for near-memory acceleration of deep ConvNets:

**Zig-zag data layout:** With the conventional tile-oblivious data layout in DRAM, several DMA transfers are required to fetch one tile. This can degrade performance due to inefficient use of DRAM bandwidth (also given that HMC uses closed-policy with low-interleaved addressing [40]). To address this problem, we modify the underlying storage of the intermediate layers in DRAM into a zig-zag form (illustrated in Figure 3c,e). This way with a single large DMA transfer request, the whole tile can be fetched by the processing cluster. This improves DRAM read performance which is critical for

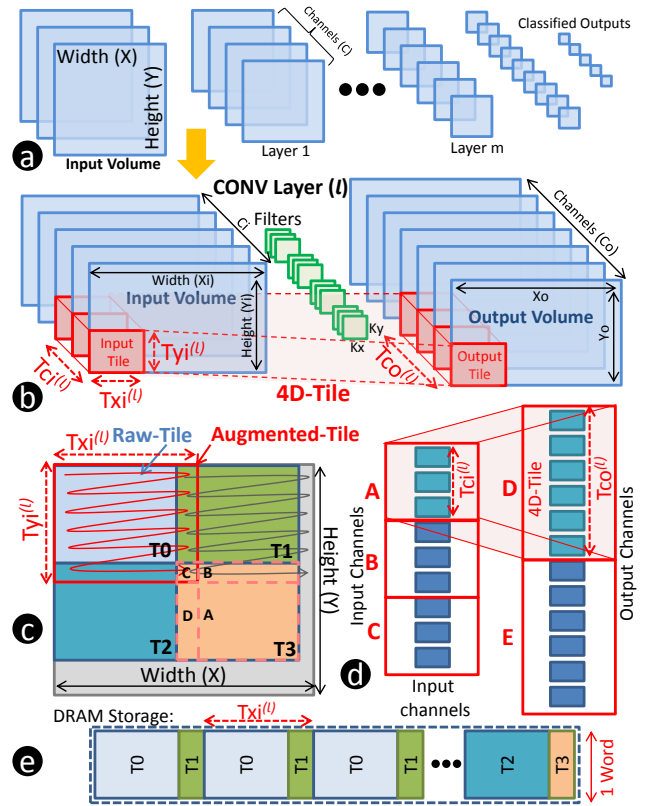


Fig. 3. (a) Illustration of a general ConvNet, (b) a 4D-tile, (c) zig-zag ordering and tile-overlapping, (d) partial computation of tiles, and (e) the underlying DRAM storage of one augmented-tile.

the proposed 4D-tiling mechanism. The implications of this mechanism on DMA write and its overheads will be explained later in this section.

**Tile overlapping:** For convolution filters larger than  $1 \times 1$ , borders of each tile need to be fetched from DRAM multiple times. Assuming that the bandwidth overhead of these overlapping regions can be tolerated by proper choice of tile dimensions, still the storage impact on the zig-zag data placement in DRAM is not trivial, and many DMA transfers might be required to implement it. This problem can be solved by storing the overlapping regions in the DRAM once per each tile. This means storing the “augmented-tiles” instead of “raw-tiles” inside DRAM in the zig-zag form, at the cost of increased DRAM storage and bandwidth. This is illustrated in Figure 3c. When reading from DRAM, a whole tile (including all overlapping regions required to compute the convolution in the borders) can be fetched using one DMA transfer request. But, when writing the results back to the DRAM some care should be taken to convert the raw output tile to an augmented-tile for the next layer (explained below). The average increases in DRAM bandwidth and storage incurred by this mechanism were found to be less than 10% and 3%, respectively. Also, on the average around 200 MB of DRAM was used with maximum usage of 580 MB for ResNet with 4M-pixel images.

**Partial Computations:** Tiling of channels ( $T_{C_i}^{(l)}$  and  $T_{C_o}^{(l)}$ ) requires maintaining partial computations, as more than one input tile contribute to the result of each output tile. For this

reason, assuming that one input tile and one output tile can fit in each cluster’s SPM, we perform the following steps to compute each output tile: Tile  $A$  (See Figure 3d) and the related filter coefficients ( $K_{AD}$ ) are fetched from the DRAM. Then,  $D = D + A * K_{AD}$  is computed inside the SPM ( $D$  containing partial sums of the output channels). Next, Tile  $B$  and  $K_{BD}$  are fetched from the DRAM, and  $D = D + B * K_{BD}$  is computed, and so forth. After all input tiles have been read once, activation and pooling are directly performed on the output tile  $D$  (again inside the SPM) and then the resulting output tile is written back to the DRAM by the PEs. This mechanism reduces DRAM’s write bandwidth and puts more pressure on read bandwidth, depending on the ratio between  $T_{C_o}^{(l)}$  and  $T_{C_i}^{(l)}$ . In all the experiments of this paper, DRAM’s write bandwidth was found to be less than 4% of the read bandwidth. This suits our tile-overlapping mechanism (requiring DRAM writes to be off the execution critical path).

It is important to explain how DRAM writes are handled, given that each output tile will be eventually the input tile of another layer, and data cannot be magically reorganized in the DRAM. Since DRAM’s write bandwidth is significantly lower than the read bandwidth (as explained above). In each DRAM write phase multiple small DMA transfers illustrated in Figure 3e are used to convert the raw output tile (currently stored in the SPM) to an augmented input tile of the next layer (Figure 3c). Therefore, each tile is reorganized during the DRAM write phase in such a way that the next DRAM read phase can fetch it with a single DMA request. Another key point is that the raw-tile width and height of the adjacent layers must be equal (for consistent zig-zag data layout), unless there has been a strided-convolution [2] or pooling stage between them, for which the tile dimensions will shrink. This way, as we move forward through the ConvNet layers, tile width and height ( $T_{X_i}^{(l)}$ ,  $T_{Y_i}^{(l)}$ ) tends to shrink. To avoid this having a negative impact on computation and SPM usage efficiency, we need to increase  $T_{C_o}^{(l)}$  or  $T_{C_i}^{(l)}$ . This completely modifies the shape and number of the tiles in each layer and impacts everything from synchronization overheads to efficiency of the computing loops and DRAM bandwidth. This highlights the need for a flexible computing cluster to support a wide range of tile dimensions.

### B. Mapping Tiles to Clusters

Since there is no data overlap among augmented-tiles (except possibly for some filter coefficients), each cluster executes one tile at a time. This minimizes communication among the clusters. Also, tiling information is prepared off-line (only once) and is stored in a list accessible by all clusters. Each cluster, when idle from its previous job, consults this list to obtain the required information (e.g. address in DRAM, size, and filter coefficients) for the next tile. This way the computation load is automatically balanced among the clusters. This procedure continues until all tiles in a layer are finished. At this point, all clusters are synchronized before proceeding with the next layer. Inside each cluster the master PE (the first PE in each cluster) partition the tile among the

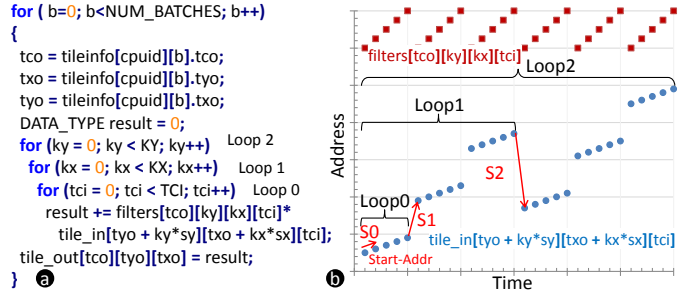


Fig. 4. (a) A convolution kernel to be performed on a 4D-tile, (b) a typical memory access pattern generated by this kernel.

NSTs in the order of  $T_{C_o}^{(l)}$ ,  $T_{X_o}^{(l)}$ , and  $T_{Y_o}^{(l)}$  dimensions first, as their outputs become independent (No need for synchronization). If still more NSTs are remaining,  $T_{C_i}^{(l)}$  is used for tile partitioning, posing some synchronization overheads to the PEs. Corner tiles (with smaller dimensions) and arbitrary sized-tiles are properly handled in this scheme. Thanks to this tile-mapping mechanism, NSTs can work independently without worrying about getting synchronized with each other. Any required synchronization is handled by the RISC-V PEs, through hardware primitives devised for this purpose. Given that  $(X_o \times Y_o \times K_x \times K_y \times C_i \times C_o)$  MAC operations need to be done in each layer (See Figure 3b), 4D-tiling can be viewed as a schedule (in time and space) of this computation to the available resources in NeuroCluster. Each cluster works based on ping-pong buffering to hide the setup and DMA transfer latencies. While one tile is being computed by the NSTs in each cluster, another tile is being fetched by the master PE, and tiling information is being prepared for it.

Overall, the computation inside each SMC is done in a self-contained manner, without consulting the host processors. The user only offloads a ConvNet task to the SMC, and the rest of the computation happens completely inside the cube. The serial-links are turned-off when not required to save energy. The advantages of this mechanism on performance and energy are studied in subsection VI-C.

## V. PROGRAMMING MODEL

A light-weight and flexible API is developed along with a standard device-driver, exposing PIM’s capabilities to user-level applications running on the host processors. This software stack is developed based on parallel programming APIs and is compatible with standard accelerators (e.g. GPUs). It allows users to offload complete ConvNet tasks to PIM, relieving them from the burden of programming and coordinating the NeuroClusters. Software stack is outside the scope of this work and can be found in [44].

Inside each processing cluster, the master PE is responsible for instructing the DMA engine to load/store the tiles from DRAM, and for programming the NSTs to perform the actual computations. The available SPM inside each cluster is divided into two sections (each enough to fit the largest possible tile). While one tile is being computed by the NSTs, the other one is being transferred to/from DRAM by cluster’s DMA. This way communication latency is hidden behind computation

```

a
For k=0; k<E2; k++;
  For j=0; j<E1; j++;
    For i=0; i<E0; i++;
      ACC +=
        TCDM[AGU0] × TCDM[AGU1]
      AGU0 += S0
      AGU1 += S10
    AGU0 += S01
    AGU1 += S11
  AGU0 += S02
  AGU1 += S12

b // Once per batch
ISSUE-CMD(MEM-LDC, AGU0-S0, 1);
ISSUE-CMD(MEM-LDC, AGU0-S1, TCI*(Sx-1));
ISSUE-CMD(MEM-LDC, AGU0-S2, TCI*(TXI*Sy-Sx*KX+1));
ISSUE-CMD(MEM-LDC, AGU1-S0, 1);
ISSUE-CMD(MEM-LDC, AGU1-S1, 0);
ISSUE-CMD(MEM-LDC, AGU1-S2, 0);
ISSUE-CMD(NST0, MEM-LDC, HWL-E0, TCI);
ISSUE-CMD(NST0, MEM-LDC, HWL-E1, KX);
ISSUE-CMD(NST0, MEM-LDC, HWL-E2, KY);
// Once per stream
ISSUE-CMD(NST0, MEM-LDC, AGU0-A, &kernels[tc0][0][0]);
ISSUE-CMD(NST0, MEM-LDC, AGU1-A, &tile_in[ty0][tx0]);
ISSUE-CMD(NST0, STREAM-MAC, 0, 0);

```

Fig. 5. (a) The implementation of the *STREAM\_MAC* command inside the NSTs, and (b) the required set of commands to program it to do so.

as much as possible. subsection V-A describes how NSTs are programmed by the PEs to perform the tasks related to forward-propagation in ConvNets. subsection V-B presents the implementation of back-propagation and training on the NSTs.

### A. Programming the NSTs for Forward-propagation

Figure 4a illustrates a convolution kernel to be performed on a 4D-tile. *Filters* and *tile\_in* are the two data structures accessed in every iteration of the inner-loop. Typical memory access patterns for this kernel are plotted in Figure 4b. These patterns seem fairly regular, therefore, NSTs should be easily able to generate them. It is enough to program the configurations registers of an NST (shown in Figure 2) with the starting address and the three step values illustrated in Figure 4b ( $S_0$ ,  $S_1$ , and  $S_2$ ), and then issue a *STREAM\_MAC* command to it. The implementation of the *STREAM\_MAC* command is illustrated in Figure 5a. Once the command is received by the main-controller in NST, it runs the nested loops in several iterations, and calculates the MAC result in the ACC register. Two SPM reads are performed every cycle on the two memory ports and the AGUs are incremented/decremented with the programmed steps. NSTs do not lose any cycles and can obtain a high computational efficiency (See subsection VI-A for results). To implement the convolution kernel shown in Figure 4a, it is enough for the PEs to issue the set of commands illustrated in Figure 5b. The latency overheads of these commands are hidden by having multiple NSTs and filling up their command queues with multiple commands.

Similarly, each NST is able to perform ReLU activation [3] on arbitrary tiles using *STREAM\_MAX* command devised for this purpose on the same set of state machines and hardware blocks (with a similar mechanism illustrated in Figure 5a). For the sake of generality, *STREAM\_SUM*, *STREAM\_SCALE*, *STREAM\_SHIFT*, and *STREAM\_MIN* are implemented, as well. Another widely used operation in ConvNets is pooling [1]. NST supports max-pooling [70] through the *STREAM\_MAXPL* command shown in Figure 6a. Thanks to the flexibility of the AGUs and HWLs, arbitrary tiles with different pooling strides are supported. This way ConvNets of different sizes can be easily executed on this platform in a scalable fashion.

### B. Implementation of Back-propagation

Back-propagation is the prevalent method for training NNs including ConvNets [2]. In this mechanism, given a set of

```

a For k=0; k<E2; k++;
  ACC=0
  For j=0; j<E1; j++;
    For i=0; i<E0; i++;
      ACC = Max{ACC, SPM[AGU0]}
      AGU0 += S0
      AGU1 += S10
    AGU0 += S01
    AGU1 += S11
  SPM[AGU1] = ACC
  AGU0 += S02
  AGU1 += S12

b For k=0; k<E2; k++;
  ACC=0
  For j=0; j<E1; j++;
    For i=0; i<E0; i++;
      ACC += TCDM[AGU0] × TCDM[AGU1]
      AGU0 += S0
      AGU1 += S10
    AGU0 += S01
    AGU1 += S11
  SPM[AGU1] = ACC
  AGU0 += S02
  AGU1 += S12

```

Fig. 6. The implementation of (a) *STREAM\_MAXPL* and (b) *STREAM\_GD* commands inside the NSTs.

training sample inputs, first a forward propagation is executed layer-by-layer, then using an optimization algorithm such as gradient descent (GD) [1] the coefficients (weights) are updated backwards so that the network learns that sample. the forward pass can be performed exactly as described in the previous sections, but the back-propagation requires implementing GD. Different forms of GD optimization are supported by the NSTs. A simple implementation obtained from a real ConvNet [71] [72] is shown here, where  $W$  stands for weights (coefficients) and  $dW$  stands for the differences obtained from back-propagation:

$$\begin{aligned}
 & \text{for } i \text{ in range}(W.len) : \\
 & \quad W_i = W_i - \alpha(dW_i + \lambda W_i);
 \end{aligned}$$

The main body of this loop can be rewritten as:

$$\begin{aligned}
 W_i &= (1 - \lambda \alpha) W_i - \alpha dW_i \\
 W_i &= C_0 W_i + C_1 dW_i
 \end{aligned}$$

where,  $C_0$  and  $C_1$  are calculated and stored in the SPM, once per each batch of tiles. More generally, NSTs are able to compute the following formula through the implementation illustrated in Figure 6b:

$$W_i = \sum_{j=0}^{n-1} C_j \cdot W_i^{(j)} \quad (1)$$

where  $W_i^{(j)}$  is the j-th derivation of  $W_i$ . This is enough to support a wide range of GD algorithms, including Stochastic GD (SGD) [73], and batch GD (BGD), even on 2D surfaces. It should be noted that the AGU steps can also be negative. This way by some programming effort, complex nested loops over multi-dimensional arrays can be implemented by NSTs. Detailed implementation of parallel training on our PIM platform is an ongoing work, nevertheless, subsection VI-A also presents an estimation for the training performance on this platform, showing that a high efficiency is achievable for training, as well.

## VI. EXPERIMENTAL RESULTS

This section presents the experimental results obtained with the proposed PIM platform. Our baseline system is composed of a memory-centric network [74] of four SMC devices based on a mesh topology. Each SMC hosts a NeuroCluster with 16 clusters on its LoB die, with each cluster having 4 RISC-V cores (with 1KB private instruction cache each), 8 NSTs,



a DMA engine, and 128KB of SPM. This configuration is found to achieve reasonable performance and efficiency through several simulations. Total available DRAM is 1GB in 4 stacked dies with DRAM banks of 32MB and a closed-page policy [43]. Low-interleaved-addressing is implemented as the HMC’s default addressing scheme [40]. A summary of these parameters is also listed in Figure 1b. A fully functional and cycle-accurate (CA) RTL model of the NeuroCluster has been modeled in SystemVerilog, with the components adopted and reconfigured from [68]. This model along with a previously developed cycle-accurate model of the SMC [43] allows us to analyze the performance of tiled execution over a single SMC device considering the programming overheads. Silicon area and power consumption are also extracted from these models using topographical logic synthesis (See subsection VI-B).

In addition, an epoch-based in-house simulator is developed (modeling the SMC network illustrated in Figure 1a) to estimate the performance and power consumption of executing full ConvNets on large images, based on the data obtained from the CA simulations. This strategy allows us to obtain both reasonable accuracy and very high simulation speed. Our simulation platform supports CAFFE [19] representation of the SoA ConvNets. For every layer of the ConvNets under study the optimum tile dimensions are found based on performance, energy efficiency, available SPM size, and required DRAM bandwidth. This procedure requires multiple simulations with different combinations of parameters, and is only done once per each ConvNet (at the beginning). Optimally sized tiles can then be used in later simulations with different images. Four serial link controllers in LoB are modeled to consume up to 10 W of power for highest traffic pressure [44] [75]. We can share this 10 W power budget between the serial link controllers and NeuroCluster, and for example by turning off one of them we give a 2.5 W power budget to NeuroCluster allowing it to operate in the “shadow” of a powered-down serial link. Performance is studied in subsection VI-A. Detailed energy consumption and silicon area results are presented in subsection VI-B. Finally, the overall results of the multi-SMC network are presented in subsection VI-C.

### A. Performance of Single SMC

The average GFLOPS efficiency of a single cluster measured in CA simulation is illustrated in Figure 7. The cluster is executing tiled convolutions (Figure 4a) with 1x1, 2x2, and 3x3 filters and typically sized tiles on all its NSTs. The banking-factor<sup>2</sup> (BF) of the scratchpad memory is changed from 1/4 to 4 (i.e. from 4 to 64 banks). On the average, BF=2 yields an efficiency of over 93% for the execution of a single tile. This is why the baseline cluster illustrated in Figure 1 features 32 SPM banks. Moreover, execution efficiency reduces as the convolution filters shrink (3x3 > 2x2 > 1x1). Shrinking filter dimensions is a common trend in modern ConvNets, and will be further investigated later in this section.

<sup>2</sup>Banking-factor is the ratio between the number of SPM banks and the number of master ports (from the NSTs). In WLI memories, this parameter directly affects the ratio of bank-conflicts inside the SPM, and has a critical impact on the clock frequency and area of the cluster interconnect. More information: [76]

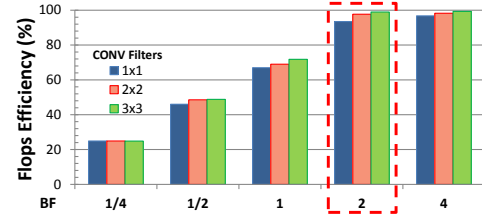


Fig. 7. The effect of SPM’s banking-factor on the average GFLOPS efficiency of a single cluster, executing tiled convolutions with 1x1, 2x2, and 3x3 filters and typically sized tiles on its NSTs

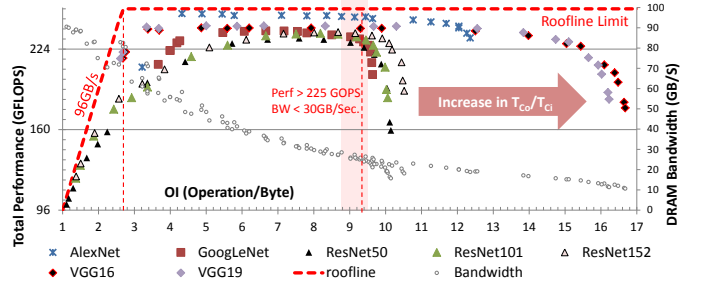


Fig. 8. Roofline plot for execution of the full ConvNets over a single SMC device along with DRAM bandwidth.  $T_{Co}^{(l)}/T_{Ci}^{(l)}$  of all layers are altered to obtain different OI ratios.

Another point is that a traditional bank-level interleaved (BLI) SPM needs to be explicitly managed and partitioned by software, and its performance is highly dependent on the tile dimensions. A significant amount of bank-conflicts can occur if it is not properly managed. Also with BLI, only half of the banks will be used for computation (because of ping/pong buffering), further reducing the bandwidth. Therefore, in this paper we choose WLI instead because of its flexibility and high parallelism regardless of the tile dimensions.

Figure 8 illustrates the roofline plot [45] for complete execution of the ConvNets listed in Table I on a single SMC. For each ConvNet, different OI ratios are achieved by altering the tile channel ratios of all layers ( $R_{TCL} = T_{Co}^{(l)}/T_{Ci}^{(l)}$  is directly proportional to OI). Left axis shows achievable GFLOPS, and right axis shows the average DRAM bandwidth. This plot highlights the importance of proper tile sizing on delivered performance, as different ConvNets have different optimal points. Also, too much increase in  $R_{TCL}$  can negatively impact performance, because the initialization overhead of the NSTs is highly dependent on this parameter, especially for ResNet with a high percentage of 1x1 filters (as later explained in this section). An average DRAM bandwidth of 32 GB/s was found enough for all ConvNets under study, yet, to support larger bandwidth demands and allow for smooth operation under momentarily large bandwidth demands, we have dedicated 3 AXI ports to the global-interconnect shown in Figure 1, summing to a maximum of 96 GB/sec.

Having found the optimum tile dimensions for each ConvNet, Figure 9a depicts the overall performance (GFLOPS) and total execution time for the studied ConvNets on a single cube. VGG networks have the highest execution time, due to their higher requirement for MAC operations, while GoogLeNet and AlexNet are the fastest ones executing in less than 12 ms.

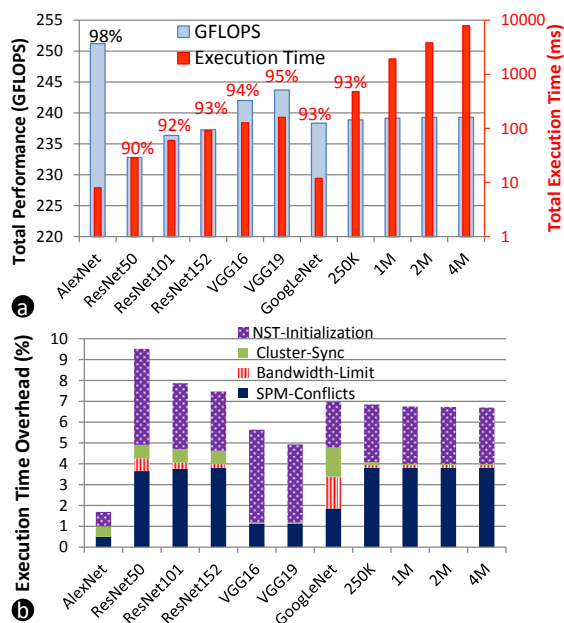


Fig. 9. (a) Performance comparison of different ConvNets on a single SMC device, and (b) breakdown of different overheads contributing to performance loss.

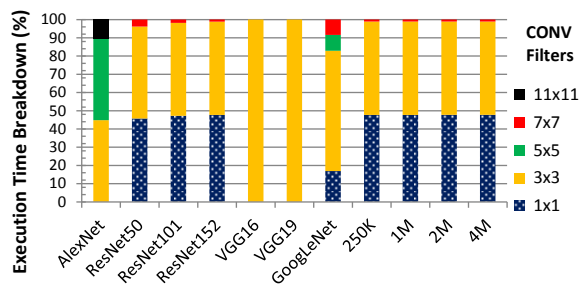


Fig. 10. Breakdown of total execution time versus the size of the convolution filters.

GoogLeNet has a very low computation requirement (less than 2 GMAC for each forward pass) compared to the other modern networks (ResNet and VGG) mainly due to the use of strided-convolution in the beginning layers. It can be further seen that the ResNet group achieve the lowest GFLOPS efficiency. This can be associated with higher percentage of SPM conflicts illustrated in Figure 9b. This figure also shows different sources contributing to the performance loss of each ConvNet. In order to understand this plot better, a breakdown of total execution time is plotted in Figure 10a versus the size of the convolution filters. As can be seen, a significant portion of the execution time (over 45%) of the ResNet group is spent in 1x1 filters, and as we saw previously in Figure 7, 1x1 filters cause more SPM conflicts than larger filters. Plus, for 1x1 filters the 3 convolution loops illustrated in Figure 4a change into a single loop iterating over  $T_{c_i}$ . This increases the relative overhead of NST initialization (shown in Figure 9b).

To demonstrate the scalability of the proposed PIM platform, the size of the input images is increased from 250K-pixels to 32M-pixels, and execution-time per pixel with execution overheads for ResNet are plotted in Figure 11. This

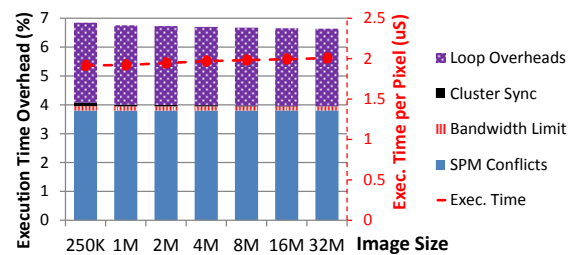


Fig. 11. Execution overheads (left-axis), and execution-time per pixel versus image size for ResNet-based networks (right-axis).

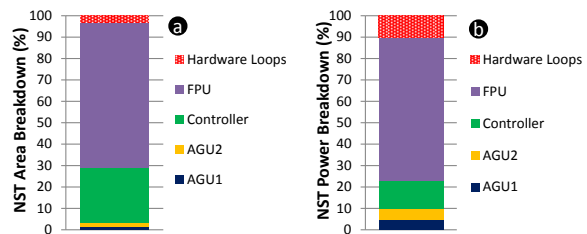


Fig. 12. Area and power breakdown inside one instance of NeuroStream.

plot clearly shows that the execution overheads do not increase even for very large images, and execution-time per pixel only increases slightly due to the increased number of layers. This proves the effectiveness of the proposed 4D-tiling mechanism and the efficient programming paradigm based on ping-pong buffering to hide the latencies. To summarize each SMC instance is capable of processing 126, 83, 34, 16, 11, 8, 6 frames (each frame being  $220 \times 220 \times 3$  Bytes) per second for AlexNet, GoogLeNet, ResNet50, ResNet101, ResNet152, VGG16, VGG19, respectively, with an average performance of 240 GFLOPS. This performance is scalable to larger images as Figure 11 demonstrates.

Lastly, an estimation of the training performance can be obtained as follows. One forward pass of ResNet152 and GoogLeNet takes 90 mS and 11 mS, respectively, and they have a total of 211 MB and 4 MB of coefficients. Based on the code illustrated in Figure 6b and estimated initialization and synchronization overheads, a backward pass takes less than 3 mS for ResNet152 and less than 0.1 mS for GoogLeNet. This suggests that back-propagation can be implemented efficiently, as well, using our PIM system with a performance drop of less than 5%.

### B. Silicon Area and Power Efficiency

A complete processing cluster shown in Figure 1b was synthesized using Synopsys Design Compiler (J-2014.09-SP4) in topographical mode in 28nm FDSOI technology of STMicroelectronics (1.0V, SS, 125°C, Low Threshold Voltage Transistors), achieving a clock frequency of 1GHz. Power consumption was extracted using Synopsys Primetime (H-2013.06-SP2) at 25°C, TT, 1.0V. The CA cluster model runs the tiled-convolution illustrated in Figure 4a on typical tiles by offloading them to its NSTs similar to Figure 5b. Switching activity is then recorded and fed to Primetime for power extraction. For vault controllers and the SMC controller previously developed models in [43] and [44] were used (all in

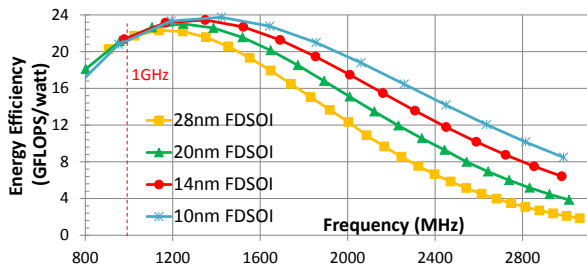


Fig. 13. Effect of technology scaling of the LoB die on the energy efficiency of a complete SMC device. Voltage is scaled to achieve different operating frequencies.

28nm FDSOI), the serial link area and energy were estimated based on [75] [77]. 5000 TSVs [78] with a pitch of  $48 \mu\text{m} \times 55 \mu\text{m}$  [79] were used to estimate TSV matrix area, with energy modeled from [75].

Figure 12 illustrates the power and area breakdown inside one NST instance. As expected, over two-third of the total power and area are dedicated to the streaming FPU's depicted in Figure 2, while the controller accounts only for 26% of the total area and 13% of the power consumption. These simplified state-machines allow for a significant energy reduction compared to full-featured processors such as RISC-V (see below). Figure 14 illustrates the area and power breakdowns for a complete cluster of Figure 1b, where the number of cores is changed. Decreasing the number of RISC-V core from 8 to 4 gives an average power and area reduction of 20% and 22%, respectively, while from 4 to 2 smaller reductions of 10% and 13% are obtained. Reminding that having fewer RISC-V cores increases the programming overheads (each core needs to manage more NSTs), we choose to have 4 cores per cluster. For the NSTs, 8 instances was found optimal, as beyond that the delay and area of the cluster-interconnect limits achievable frequency. The optimal SPM size in terms of energy-efficiency was found to be 16KB per NST. This is shown in Figure 15a, yielding 22.5 GFLOPS/W and 2.7 GFLOPS/W/mm<sup>2</sup>. This is for a total of 16 clusters, while having more clusters negatively impacts the area-efficiency and yields diminishing energy returns (See Figure 15b). Furthermore, 16 clusters occupy only 8% of the total LoB die (as explained below). Therefore, the die alignments are not perturbed. This is while too much increase in the LoB die area not only increases silicon cost, but also complicates the packaging and alignment, deviating from the standard HMC devices. The optimal parameters found in this section are listed in Figure 1b and used in all experiments.

The choice of a moderate operating frequency in our design is justified through the experiment shown in Figure 13 for different technology choices. In this figure, the energy efficiency of a complete SMC device executing different ConvNets is estimated for the 28nm to 10nm FDSOI technologies at various operating points. Interestingly, a moderate clock frequency of 1.2GHz achieves the highest efficiency, and increasing the clock speed beyond that is not beneficial. This is mainly due to the communication bound (DRAM's latency and bandwidth), limiting the achievable performance. This choice, also, relieves us from thermal concerns. As in [52] a 3D thermal simulation of the HMC with 4 stacked DRAM

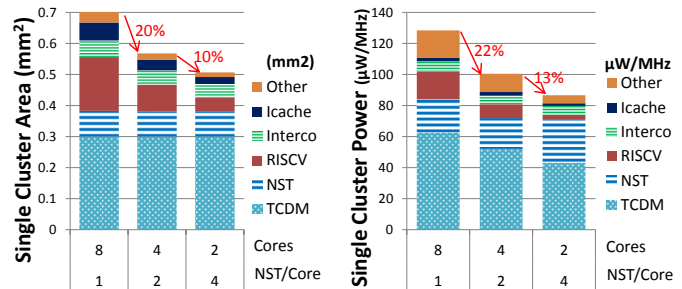


Fig. 14. Area and power breakdown for one of the clusters shown in Figure 1, where the number of cores has been changed from 2 to 8

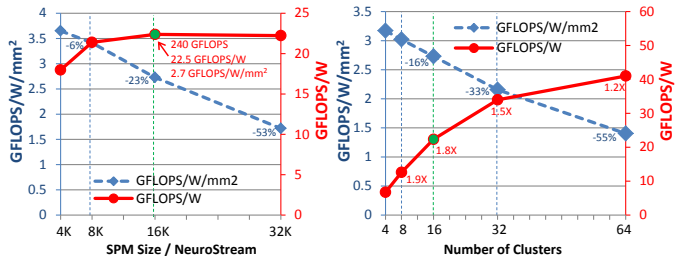


Fig. 15. (a) Effect of the SPM size per each NST and (b) the number of total clusters, on energy and area efficiency of the SMC.

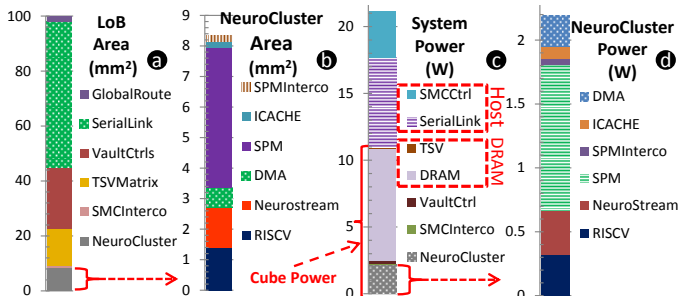


Fig. 16. (a) Silicon area of the whole LoB die and (b) one NeuroCluster. (c) Total system power for NeuroCluster placed on the host side, (d) power breakdown inside NeuroCluster.

dies shows that a processing cluster clocked up to 5 GHz can be embedded in its LoB die increasing the temperature up to  $76^\circ\text{C}$  which is below the thermal limits of HMC [40]. Power consumption is a secondary concern, as well, because up to 10W budget is available in the LoB die by turning-off the serial links, and NeuroCluster consumes 2.2W.

Figure 16c illustrates different contributors to power consumption in the baseline configuration. *Cube Power* represents the total consumed power inside a single SMC averaged for the execution of all ConvNets under study. As can be seen 11W is consumed inside the cube, on the average. The NeuroCluster is responsible only for 2.2W of this power. While the rest (around 75%) is consumed inside the DRAM dies. The power consumed in NeuroCluster is dominated by the Scratchpad Memory (51%) and the NSTs (16%), while the RISC-V cores only consume 14% (See Figure 16d). This highlights the efficiency of this architecture, minimizing the unnecessary power consumed in control-flow and dedicating it to the computations. Each NST instance consumes an average of 2.7 mW, while a RISC-V core consumes 2.2 mW

just for programming and coordinating the NSTs. Overall, an energy efficiency of 22.5 GFLOPS/W is achieved inside one SMC for the execution of complete ConvNets (NeuroCluster itself achieves 117 GFLOPS/W). Moreover, the best off-the-shelf GPU can achieve 4.6 GFLOPS/W with disabled error-correcting-codes (ECC), boosted clock, and advanced ConvNet implementations techniques [30]. This is 4.9X worse than the efficiency achieved by a single SMC.

Another interesting observation is that if we place the NeuroCluster accelerator on the host side (behind the SMC controller and the serial links) rather than inside the SMC, while maintaining exactly the same computation paradigm, the total execution time and the power consumed in the NeuroCluster itself do not change much, but on the average, system power increases by 10.2 W. This power is consumed in the SMC controller and the serial links, suggesting that computing inside the SMC can give an average energy reduction of 48% compared to a similar host-side accelerator (1.7X improvement in system-level energy efficiency). Finally, looking at the silicon area results in Figure 16a,b we can see that the NeuroCluster (8.3 mm<sup>2</sup>) occupies around 8% of the area in the LoB die with the SPM (55% of NeuroCluster), the RISC-V cores (16.5%), and the NSTs (16%) being the main contributors. The total area for the LoB die was estimated as 99 mm<sup>2</sup>.

### C. The Multi-SMC Network

This section presents the estimated performance and energy efficiency for the SMC network illustrated in Figure 1a. Four SMC devices are connected to each other using mesh topology with an HD camera recording raw images of 8M-pixels. The camera sends the images to the memory cubes over the highlighted links in Figure 1a, and each SMC executes ResNet on one complete image, independently from the other cubes. Each SMC has a copy of the ConvNet coefficients inside its DRAM dies, and the coefficients have been preloaded once at the beginning. The host system-on-chip (SoC) is only responsible for coordination and receiving the results. It does not send or receive data at a high bandwidth, yet we keep its serial link (Link0) always active, to make sure it can manage the other devices through that link. The other serial links, however, are turned on only when there is a data to send over them, and then turned off again. Considering a typical bandwidth of 16 GB/sec for each serial link, and the power-state transition times obtained from the HMC specifications V2.1 [40] [Active to Sleep: 600 ns ( $t_{SME}$ ), Sleep to Power-Down: 150  $\mu$ s ( $t_{SD}$ ), and Power-Down to Active: 50  $\mu$ s], the total power consumed in the SMC network can be estimated as 42.8 W. The camera sends images to the cubes in a ping-pong fashion: while an SMC is working on one image, the camera sends another image to its DRAM. This is easily achievable because there is plenty of space available inside each SMC.

This architecture is compared with NVIDIA Tesla K40. This GPU is able to achieve 1092 GFLOPS at about 235 W [30]. Our SMC network can achieve 955 GFLOPS @ 42.8 W, with 4.8X better energy efficiency. Moreover, this architecture is scalable to a larger number of nodes because the average

bandwidth demand over the serial links is not large (in the order of 10 MB/sec per image). Therefore it is possible to turn on a link, transfer the image at a higher bandwidth, and turn it off, periodically. This asynchronous and on-demand mechanism allows us to achieve a scalable performance with high energy efficiency.

### D. Opportunities for Further Improvements

The energy efficiency can be further increased by using various “application specific” enhancements, like specialized vectors, specialized line-buffers replacing normal register-files to reduce SPM access pressure, and reduced precision arithmetic. For example, reduced precision has the potential to reduce NST’s power consumption up to 70% (as shown in Figure 12b). This, itself, can result in 11% reduction in the overall cube power. Furthermore, a significant storage and bandwidth reduction can be achieved by weight binarization [80] and reduced bit-width [81]. Another point is that a significant amount of energy is consumed in the unused DRAM pages (e.g. ResNet152 uses only 23% of the available DRAM). This suggests that for larger images and networks better efficiency can be achieved within the same power budget. Also, by using more advanced refresh and power-down management schemes it should be able to reduce the consumed power in the unused DRAM pages. Finally, having multiple HMC devices, as presented in subsection VI-C, can be another scalable solution to reach the performance of high-end GPUs with a much higher energy efficiency.

## VII. CONCLUSIONS AND ONGOING WORK

In this paper, we proposed a scalable and energy-efficient PIM system based on a network of multiple SMC devices. Each SMC is augmented with a flexible clustered multi-core called NeuroCluster, capable of executing full-featured deep ConvNets with growing memory footprints and computation requirements. The key component of this architecture is NeuroStream, a streaming floating-point co-processor designed for this purpose. In addition, an efficient tiling mechanism along with a scalable programming paradigm were proposed to facilitate this operation. Our proposal requires only 8% of the total LoB die area in a standard HMC, and achieves an average performance of 240 GFLOPS for complete execution of full-featured modern ConvNets within a power-budget of 2.5 W. 22.5 GFLOPS/W energy efficiency is achieved in a single HMC which is 5X better than the best off-the-shelf GPU implementation. The performance was shown scalable to 955 GFLOPS, on par with the most powerful GPUs available today, with a small network of SMCs. It is worth stressing that our platform allows for offloading the ConvNet tasks completely into the memory cubes at a minor system power cost. This implies that the compute logic in the host SoC is free to deal with other workloads. Also, the cost increase with respect to a baseline HMC system would be negligible. Therefore, essential ConvNet acceleration is provided at a very small system cost. Ongoing research efforts include silicon implementation of the NeuroCluster with 4 clusters, parallel

implementation of back-propagation and training on this architecture, and pushing further to achieve higher performance and efficiency inside the cubes.

## REFERENCES

- [1] S. Srinivas, R. K. Sarvadevabhatla, K. R. Mopuri *et al.*, “A taxonomy of deep convolutional neural nets for computer vision,” *Frontiers in Robotics and AI*, vol. 2, p. 36, 2016.
- [2] J. Gu, Z. Wang, J. Kuen *et al.*, “Recent advances in convolutional neural networks,” *CoRR*, vol. abs/1512.07108, 2015. [Online]. Available: <http://arxiv.org/abs/1512.07108>
- [3] S. An, F. Boussad, and M. Bannamoun, in *ICML*, pp. 514–523.
- [4] N. Srivastava, G. E. Hinton, A. Krizhevsky *et al.*, “Dropout: a simple way to prevent neural networks from overfitting,” *Journal of Machine Learning Research*, vol. 15, no. 1, pp. 1929–1958, 2014.
- [5] L. Cavigelli, M. Magno, and L. Benini, “Accelerating real-time embedded scene labeling with convolutional networks,” in *2015 52nd ACM/EDAC/IEEE Design Automation Conference (DAC)*, 2015.
- [6] K. Simonyan and A. Zisserman, “Very deep convolutional networks for large-scale image recognition,” *CoRR*, vol. abs/1409.1556, 2014. [Online]. Available: <http://arxiv.org/abs/1409.1556>
- [7] Y. Han and K. Lee, “Acoustic scene classification using convolutional neural network and multiple-width frequency-delta data augmentation,” *CoRR*, vol. abs/1607.02383, 2016. [Online]. Available: <http://arxiv.org/abs/1607.02383>
- [8] S. E. Kahou, C. Pal, X. Bouthillier *et al.*, “Combining modality specific deep neural networks for emotion recognition in video,” in *Proceedings of the 15th ACM on International Conference on Multimodal Interaction*, ser. ICMI '13, 2013, pp. 543–550.
- [9] X. Li, Y. Zhang, M. Li *et al.*, “Deep neural network for RFID-based activity recognition,” in *Proceedings of the Eighth Wireless of the Students, by the Students, and for the Students Workshop*, ser. S3, 2016, pp. 24–26.
- [10] R. Adolf, S. Rama, B. Reagen *et al.*, “Fathom: Reference workloads for modern deep learning methods,” *CoRR*, vol. abs/1608.06581, 2016. [Online]. Available: <http://arxiv.org/abs/1608.06581>
- [11] P. Baldi, P. Sadowski, and D. Whiteson, “Searching for exotic particles in high-energy physics with deep learning,” *Nature communications*, vol. 5, 2014.
- [12] S. Carrillo, J. Harkin, L. J. McDaid *et al.*, “Scalable hierarchical network-on-chip architecture for spiking neural network hardware implementations,” *IEEE Transactions on Parallel and Distributed Systems*, vol. 24, no. 12, pp. 2451–2461, Dec 2013.
- [13] J. Bilski and J. Smolag, “Parallel architectures for learning the RTRN and Elman dynamic neural networks,” *IEEE Transactions on Parallel and Distributed Systems*, vol. 26, no. 9, pp. 2561–2570, Sept 2015.
- [14] D. Amodei, R. Anubhai, E. Battenberg *et al.*, “Deep Speech 2: End-to-end speech recognition in English and Mandarin,” *CoRR*, vol. abs/1512.02595, 2015. [Online]. Available: <http://arxiv.org/abs/1512.02595>
- [15] C. Szegedy, W. Liu, Y. Jia *et al.*, “Going deeper with convolutions,” in *2015 IEEE Conference on Computer Vision and Pattern Recognition (CVPR)*, June 2015, pp. 1–9.
- [16] Y. Taigman, M. Yang, M. Ranzato, and L. Wolf, “DeepFace: Closing the gap to human-level performance in face verification,” in *Proceedings of the 2014 IEEE Conference on Computer Vision and Pattern Recognition*.
- [17] T.-Y. Lin, M. Maire, S. Belongie *et al.*, *Microsoft COCO: Common Objects in Context*. Springer International Publishing, 2014.
- [18] R. Collobert, K. Kavukcuoglu, and C. Farabet, “Torch7: a Matlab-like environment for machine learning,” in *BigLearn, NIPS Workshop*, 2011.
- [19] Y. Jia, E. Shelhamer, J. Donahue *et al.*, “Caffe: Convolutional architecture for fast feature embedding,” in *Proceedings of the 22nd ACM International Conference on Multimedia*, 2014.
- [20] S. Chetlur, C. Woolley, P. Vandermersch *et al.*, “cuDNN: Efficient primitives for deep learning,” *CoRR*, vol. abs/1410.0759, 2014.
- [21] C. Farabet, C. Poulet, J. Y. Han, and Y. LeCun, “CNP: An FPGA-based processor for convolutional networks,” in *2009 International Conference on Field Programmable Logic and Applications*, Aug 2009, pp. 32–37.
- [22] C. Zhang, P. Li, G. Sun *et al.*, “Optimizing FPGA-based accelerator design for deep convolutional neural networks,” in *Proceedings of the 2015 ACM/SIGDA International Symposium on Field-Programmable Gate Arrays*.
- [23] C. Farabet, B. Martini, B. Corda *et al.*, “NeuFlow: A runtime reconfigurable dataflow processor for vision,” in *CVPR 2011 WORKSHOPS*, June 2011, pp. 109–116.
- [24] V. Gokhale, J. Jin, A. Dundar *et al.*, “A 240 G-ops/s mobile coprocessor for deep neural networks,” in *2014 IEEE Conference on Computer Vision and Pattern Recognition Workshops*, June 2014.
- [25] P. H. Pham, D. Jelaca, C. Farabet *et al.*, “NeuFlow: Dataflow vision processing system-on-a-chip,” in *IEEE 55th International Midwest Symposium on Circuits and Systems (MWSCAS)*, 2012, pp. 1044–1047.
- [26] S. Liu, Z. Du, J. Tao *et al.*, “Cambricon: An instruction set architecture for neural network,” in *Proceedings of the 43rd Annual International Symposium on Computer Architecture*, 2016.
- [27] L. Cavigelli, D. Gschwend, C. Mayer *et al.*, “Origami: A convolutional network accelerator,” in *Proceedings of the 25th Edition on Great Lakes Symposium on VLSI*, 2015.
- [28] F. Conti and L. Benini, “A ultra-low-energy convolution engine for fast brain-inspired vision in multicore clusters,” in *Proceedings of the 2015 Design, Automation & Test in Europe Conference*.
- [29] The world’s first deep learning supercomputer in a box. [Online]. Available: <http://www.nvidia.com/object/deep-learning-system.html>
- [30] Caffe performance measurements on NVIDIA GPUs. [Online]. Available: [http://caffe.berkeleyvision.org/performance\\_hardware.html](http://caffe.berkeleyvision.org/performance_hardware.html)
- [31] L. Jin, Z. Wang, R. Gu *et al.*, “Training large scale deep neural networks on the Intel Xeon Phi many-core coprocessor,” in *Proceedings of the 2014 IEEE International Parallel & Distributed Processing Symposium Workshops*, 2014.
- [32] LeNet-5. [Online]. Available: <https://github.com/BVLC/caffe/blob/master/examples/mnist/>
- [33] W. Qadeer, R. Hameed, O. Shacham *et al.*, “Convolution engine: Balancing efficiency & flexibility in specialized computing,” *SIGARCH Comput. Archit. News*, vol. 41, no. 3, pp. 24–35, Jun. 2013.
- [34] “Empowering automotive vision with TI’s vision AccelerationPac,” White Paper, TI, 2013.
- [35] CEVA-XM4 - intelligent vision processor. [Online]. Available: <http://www.ceva-dsp.com/CEVA-XM4>
- [36] Artificial intelligence now fits inside a USB stick. [Online]. Available: <http://www.engadget.com/2016/04/28/movidius-fathom-neural-compute-stick/>
- [37] Movidius myriad 2 product brief. [Online]. Available: <http://uploads.movidius.com/1441734401-Myriad-2-product-brief.pdf>
- [38] K. He, X. Zhang, S. Ren, and J. Sun, “Deep residual learning for image recognition,” *CoRR*, vol. abs/1512.03385, 2015.
- [39] J. H. Lau, “Evolution, challenge, and outlook of TSV, 3D IC integration and 3D silicon integration,” in *Advanced Packaging Materials (APM), 2011 International Symposium on*, Oct 2011, pp. 462–488.
- [40] *Hybrid Memory Cube Specification 2.1*, Hybrid Memory Cube Consortium Std., 2015.
- [41] D. Kang, W. Jeong, C. Kim *et al.*, “256Gb 3b/cell V-NAND flash memory with 48 stacked WL layers,” in *2016 IEEE International Solid-State Circuits Conference (ISSCC)*, Jan 2016, pp. 130–131.
- [42] Z. Sura, A. Jacob, T. Chen *et al.*, “Data access optimization in a processing-in-memory system,” in *Proceedings of the 12th ACM International Conference on Computing Frontiers*, 2015.
- [43] E. Azarkhish, C. Pfister, D. Rossi, I. Loi, and L. Benini, “Logic-base interconnect design for near memory computing in the Smart Memory Cube,” *IEEE Transactions on Very Large Scale Integration (VLSI) Systems*, vol. PP, no. 99, pp. 1–14, 2016.
- [44] E. Azarkhish, D. Rossi, I. Loi, and L. Benini, *Design and Evaluation of a Processing-in-Memory Architecture for the Smart Memory Cube*. Cham: Springer International Publishing, 2016, pp. 19–31.
- [45] S. Williams, A. Waterman, and D. Patterson, “Roofline: An insightful visual performance model for multicore architectures,” *Commun. ACM*, vol. 52, no. 4, pp. 65–76, Apr. 2009.
- [46] K. He, X. Zhang *et al.*, “Identity mappings in deep residual networks,” *CoRR*, vol. abs/1603.05027, 2016.
- [47] Caffe representation of AlexNet, GoogLeNet, ResNet50, ResNet101, ResNet152 ConvNets. [Online]. Available: <http://ethereon.github.io/netscope/>
- [48] Large scale visual recognition challenge. [Online]. Available: <http://image-net.org/challenges/LSVRC/>
- [49] Caffe representation of VGG16 and VGG19 ConvNets. [Online]. Available: <https://github.com/fzliu/style-transfer/blob/master/models/>
- [50] S. Han, X. Liu, H. Mao *et al.*, “EIE: Efficient inference engine on compressed deep neural network,” in *Proceedings of the 43rd Annual International Symposium on Computer Architecture*, 2016.
- [51] T. Chen, Z. Du, N. Sun *et al.*, “A high-throughput neural network accelerator,” *IEEE Micro*, vol. 35, no. 3, pp. 24–32, May 2015.
- [52] D. Kim, J. Kung, S. Chai *et al.*, “Neurocube: A programmable digital neuromorphic architecture with high-density 3D memory,” in *Pro-*



ceedings of the 43rd Annual International Symposium on Computer Architecture, 2016.

- [53] M. Peemen, A. A. A. Setio, B. Mesman, and H. Corporaal, "Memory-centric accelerator design for convolutional neural networks," in *2013 IEEE 31st International Conference on Computer Design (ICCD)*, Oct 2013, pp. 13–19.
- [54] M. Peemen, R. Shi, S. Lal *et al.*, "The neuro vector engine: Flexibility to improve convolutional net efficiency for wearable vision," in *2016 Design, Automation Test in Europe Conference Exhibition (DATE)*, March 2016, pp. 1604–1609.
- [55] A. Haidar, J. Kurzak, and P. Luszczek, "An improved parallel singular value algorithm and its implementation for multicore hardware," in *Proceedings of the International Conference on High Performance Computing, Networking, Storage and Analysis*, 2013.
- [56] J. Gmez-Luna, I. J. Sung, L. W. Chang *et al.*, "In-place matrix transposition on GPUs," *IEEE Transactions on Parallel and Distributed Systems*, vol. 27, no. 3, pp. 776–788, March 2016.
- [57] Z. Du, R. Fasthuber, T. Chen *et al.*, "ShiDianNao: Shifting vision processing closer to the sensor," *SIGARCH Comput. Archit. News*, vol. 43, no. 3, pp. 92–104, Jun. 2015.
- [58] M. Abadi, A. Agarwal, P. Barham *et al.*, "TensorFlow: Large-scale machine learning on heterogeneous distributed systems," *CoRR*, vol. abs/1603.04467, 2016.
- [59] Rethinking computation: A processor architecture for machine intelligence. [Online]. Available: <http://nfc-2016.ieeesiliconvalley.org/wp-content/uploads/sites/16/2016/06/NFIC-2016-Nervana-Amir-Khosrowshahi.pdf>
- [60] X. Meng, J. Bradley, B. Yavuz *et al.*, "MLlib: Machine learning in Apache Spark," *J. Mach. Learn. Res.*, vol. 17, no. 1, pp. 1235–1241, Jan. 2016.
- [61] M. Grossman, M. Breternitz, and V. Sarkar, "HadoopCL2: Motivating the design of a distributed, heterogeneous programming system with machine-learning applications," *IEEE Transactions on Parallel and Distributed Systems*, vol. 27, no. 3, pp. 762–775, March 2016.
- [62] L. Xu, D. Zhang, and N. Jayasena, "Scaling deep learning on multiple in-memory processors," in *3rd Workshop on Near-Data Processing (WoNDP)*, 2015.
- [63] P. Chi, S. Li, C. Xu *et al.*, "PRIME: A novel processing-in-memory architecture for neural network computation in ReRAM-based main memory," in *Proceedings of the 43rd Annual International Symposium on Computer Architecture*, 2016.
- [64] S. Mittal and J. S. Vetter, "A survey of software techniques for using non-volatile memories for storage and main memory systems," *IEEE Transactions on Parallel and Distributed Systems*, vol. 27, no. 5, pp. 1537–1550, May 2016.
- [65] M. Gautschi, P. D. Schiavone, A. Traber *et al.*, "A near-threshold RISC-V core with DSP extensions for scalable IoT endpoint devices," *CoRR*, vol. abs/1608.08376, 2016. [Online]. Available: <http://arxiv.org/abs/1608.08376>
- [66] D. Rossi, A. Pullini, I. Loi *et al.*, "A 60 GOPS/W, -1.8 V to 0.9 V body bias ULP cluster in 28nm UTBB FD-SOI technology," *Solid-State Electronics*, vol. 117, pp. 170 – 184, 2016.
- [67] R. Banakar, S. Steinke, B.-S. Lee *et al.*, "Scratchpad memory: Design alternative for cache on-chip memory in embedded systems," in *Proceedings of the Tenth International Symposium on Hardware/Software Codesign*, ser. CODES '02, 2002, pp. 73–78.
- [68] The parallel ultra low power (PULP) processing platform. [Online]. Available: <http://www.pulp-platform.org/>
- [69] E. Azarkhish, D. Rossi, I. Loi, and L. Benini, "A modular shared L2 memory design for 3-D integration," *IEEE Transactions on Very Large Scale Integration (VLSI) Systems*, vol. 23, no. 8, pp. 1485–1498, 2015.
- [70] A. Giusti, D. C. Ciresan, J. Masci *et al.*, "Fast image scanning with deep max-pooling convolutional neural networks," *CoRR*, vol. abs/1302.1700, 2013. [Online]. Available: <http://arxiv.org/abs/1302.1700>
- [71] TinyDNN: a C++11 implementation of deep learning. [Online]. Available: <https://github.com/tiny-dnn/>
- [72] Y. Bengio, "Practical recommendations for gradient-based training of deep architectures," *CoRR*, vol. abs/1206.5533, 2012. [Online]. Available: <http://arxiv.org/abs/1206.5533>
- [73] M. Zinkevich, M. Weimer, L. Li, and A. J. Smola, "Parallelized stochastic gradient descent," in *Advances in Neural Information Processing Systems 23*.
- [74] G. Kim, J. Kim, J. H. Ahn, and J. Kim, "Memory-centric system interconnect design with hybrid memory cubes," in *Proceedings of the 22Nd International Conference on Parallel Architectures and Compilation Techniques*, ser. PACT '13, 2013, pp. 145–156.
- [75] J. Jeddelloh and B. Keeth, "Hybrid memory cube new DRAM architecture increases density and performance," in *VLSI Technology (VLSIT), 2012 Symposium on*, June 2012, pp. 87–88.
- [76] E. Azarkhish, I. Loi, and L. Benini, "A case for three-dimensional stacking of tightly coupled data memories over multi-core clusters using low-latency interconnects," *IET Computers Digital Techniques*, vol. 7, no. 5, pp. 191–199, September 2013.
- [77] H. Kimura, P. Aziz, T. Jing *et al.*, "28Gb/s 560mW multi-standard SerDes with single-stage analog front-end and 14-tap decision-feedback equalizer in 28nm CMOS," in *2014 IEEE International Solid-State Circuits Conference Digest of Technical Papers (ISSCC)*, Feb 2014.
- [78] P. M. Kogge and D. R. Resnick, "Yearly update: Exascale projections for 2013," Sandia National Laboratories, Tech. Rep. SAND2013-9229, Oct. 2013.
- [79] K. Sohn, W. J. Yun, R. Oh *et al.*, "A 1.2V 20nm 307GB/s HBM DRAM with at-speed wafer-level I/O test scheme and adaptive refresh considering temperature distribution," in *2016 IEEE International Solid-State Circuits Conference (ISSCC)*, Jan 2016, pp. 316–317.
- [80] P. Merolla, R. Appuswamy, J. V. Arthur *et al.*, "Deep neural networks are robust to weight binarization and other non-linear distortions," *CoRR*, vol. abs/1606.01981, 2016. [Online]. Available: <http://arxiv.org/abs/1606.01981>
- [81] D. Kadedotad, S. Arunachalam, C. Chakrabarti, and J.-s. Seo, "Efficient memory compression in deep neural networks using coarse-grain sparsification for speech applications," in *Proceedings of the 35th International Conference on Computer-Aided Design*.



**Erfan Azarkhish** received the B.Sc and M.Sc. degrees in Computer Engineering and Computer Architecture from the School of Electrical and Computer Engineering at the University of Tehran, Tehran, Iran in 2007 and 2009, respectively. He joined the Microelectronics Research Lab (Micrel), University of Bologna, Bologna, Italy in 2012, and received his Ph.D. degree in Electronics Engineering from the same university, in 2015. He is currently a post-doc researcher at the University of Bologna, focusing on the design and optimization of 3-D cluster-based many-core platforms, as well as, near-memory hierarchies for memory computation.



**Davide Rossi** received the Electronics Engineering degree from the University of Bologna, Bologna, Italy and M.Sc. from Tampere University of Technology, Tampere, Finland in 2007. Since 2008 he has been a consultant for STMicroelectronics, in the field of reconfigurable architectures. He received the Ph.D. degree from university of Bologna in 2012. His main research interests include VLSI system on chip design and ultra low power many core architectures.



**Igor Loi** received the B.Sc. degree in Electrical Engineering from the University of Cagliari, Cagliari, Italy, in 2005 and the Ph.D. degree in the Department of Electronics and Computer Science, University of Bologna, Italy, in 2010. He is currently holding the position of post-doc in Electronic Engineering at the University of Bologna. He is focusing his research on ultra-low power multi-core systems, memory systems evolution, and ultra low-latency interconnects.



**Luca Benini** is the Chair of Digital Circuits and Systems at ETH Zurich and a Full Professor at the University of Bologna. He has served as Chief Architect for the Platform2012/STHORM project at STMicroelectronics, Grenoble. Dr. Beninis research interests are in energy-efficient system and multi-core SoC design. He is also active in the area of energy-efficient smart sensors and sensor networks. He has published more than 700 papers in peer-reviewed international journals and conferences, four books and several book chapters. He is a Fellow of the ACM and a member of the Academia Europaea.